Processing and Application of Ceramics 18 [2] (2024) 203–212
https://doi.org/10.2298/PAC2402203M

Graded YSZ/Al_2O_3 nanocomposite coatings fabricated by electrophoretic deposition of Al and nanosized YSZ particles

Leyla Mostafapour[1], Saeid Baghshahi[1], Masoud Rajabi[1], Seyed Mahdi Siahpoosh[2,*], Fateme Esfehani[1]

[1]*Department of Materials Science & Engineering, Faculty of Technology and Engineering, Imam Khomeini International University (IKIU), Qazvin, Iran*
[2]*Department of Materials Science & Engineering, College of Technology and Engineering, Takestan Branch, Islamic Azad University, Takestan, Iran*

Received 8 November 2023; Received in revised form 4 June 2024; Accepted 18 June 2024

Abstract

Yttria-stabilized zirconia (YSZ)/Al_2O_3 composite coatings with a compositional gradient along the film cross-section were deposited on a nickel-based superalloy by electrophoretic technique and subsequent multi-step sintering route. Aluminium powder was used to reinforce the YSZ matrix by the in situ formation of alumina during the sintering procedure. The electrostatic interaction between particles in suspensions was evaluated through zeta potential and particle size analyses. Then, electrophoretic deposition (EPD) on Inconel 718 electrodes was carried out by employing three well-dispersed suspensions, including nanostructured YSZ with 0, 30 and 50 wt.% Al particles. XRD characterization indicated that tetragonal zirconia, monoclinic zirconia and alumina mainly existed in the coating after sintering at 1150 °C. Surface morphology and cross-sectional views of each layer were characterized by field emission scanning electron microscopy (FE-SEM). The elemental map analyses of the energy dispersive X-ray spectroscopy (EDS) technique confirmed that the YSZ content increases gradually across the sample cross-section. The mean thickness of the coating was about 200 µm. Particle size analysis by FE-SEM indicated that the majority of quasi-spherical YSZ particles on the surface had the size in nano-range after sintering at 1150 °C.

Keywords: *YSZ/Al_2O_3 functionally graded materials, electrophoretic deposition, thermal barrier coatings*

I. Introduction

Two well-recognized strategies for toughening ceramics are to deflect or to shield growing cracks by using secondary phases such as particles [1,2] and to introduce high residual compressive stresses by forming a laminate ceramic composite [3,4]. A possible solution for applying these strengthening mechanisms is to produce functionally graded materials (FGMs). Based on size and scale, the FGMs could be classified in the form of coatings that are applied to the surface of the material to improve their surface properties, or they could be in the form of bulk material, in which its properties are changing across the whole volume of the material [5]. The controlled modifications of the composition in FGMs can reduce the magnitude of the thermal stresses, suppress the plastic flow and cracking and improve interfacial bonding, provided that the graded microstructure is thermo-mechanically stable during loading [6].

One of the techniques to prepare planar FGMs is electrophoretic deposition (EPD). It allows forming a continuous compositional gradient by controlling the powder composition in the suspension from which particles are deposited on one of the electrodes. This technique has the advantages of simplicity, fast deposition rate, cost-effectiveness, good uniformity and no requirement of the particular shape of the substrate, which leads to a close-packed powder compact that needs sintering to achieve a fully dense deposit [7]. Therefore, EPD is a convenient technique for the controlled assembly of nanoparticles, thus, being a versatile processing tool to obtain self-standing nanoscale films and nanostructured coatings [8,9].

* Corresponding author: tel: +98 9122815694
e-mail: *sm.siahposh@gmail.com*

Thermal barrier coatings (TBCs) act as the thermal insulator to reduce the heat transfer to substrates; thereby, they can play an essential role in protecting metallic parts used at high operating temperatures such as gas turbines, while increasing the turbine inlet temperature (TIT) [10]. Improvement in power output and thermal efficiency of the gas turbine significantly depends on the increase of TIT [11,12].

Different types of coatings, such as Y_2O_3-stabilized ZrO_2 (YSZ) [12–14], alumina-based (Al_2O_3) [15–17] and rare-earth pyrochlores with $A_2^{3+}B_2^{4+}O_7$ structure such as lanthanum zirconate ($La_2Zr_2O_7$) [10,18] are currently considered as TBCs. However, YSZ coatings, due to having excellent toughness, high mechanical and erosion resistance, high melting point, low thermal conductivity, and relatively high thermal expansion coefficient, have attracted the increasing attention of scientific communities in the last few decades for applying thermal barrier coatings [12,13,19]. Al_2O_3-based ceramics offer high hardness, lower strength and a high elastic modulus [20]. The combination of high hardness and Young's modulus of the Al_2O_3 with the additional toughening effect provided by the ZrO_2, has been reported to lead to an increase in the flexural strength and fracture toughness of coatings [21]. During the last decade, YSZ-Al_2O_3 composite coatings have been considered to improve the lifetime of TBC [22]. Keyvani *et al.* [23] reported that YSZ-Al_2O_3 composite coating presented a better hot corrosion resistance than conventional YSZ coating.

A zirconia/alumina FGM has been of great interest, mainly to enhance the tensile strength and fracture toughness of the produced composite [24]. Sarkar *et al.* [25] prepared functionally gradient composites of YSZ and Al_2O_3 by EPD using suspensions based on commercially available micro-powders. A single-layer composite deposit with 3–6 mm in thickness was obtained by starting from the YSZ suspension, and a stream of the Al_2O_3 suspension was slowly and continuously injected into the bottom of the EPD bath. Kirbiyik *et al.* [26] produced Al_2O_3/CYSZ functionally graded thermal barrier coatings by atmospheric plasma spraying (APS) process on three substrates of aluminium, Inconel 625 and stainless steel. Both aluminium oxide and ceria-yttria stabilized zirconia powders used as ceramic top coating were in the scale of micro-particles. Liu *et al*. [27] investigated the preparation of a functionally graded YSZ/Al_2O_3 coating onto the surface of a YSZ substrate by a dip coating method. YSZ, layered YSZ-alumina and functionally graded YSZ-alumina TBC coatings were deposited by Saremi and Valefi [28] via atmospheric plasma spraying using agglomerated nanopowder. It was found that functionally graded YSZ-Al_2O_3 coatings had the improved performance in terms of tensile strength, thermal shock resistance and oxidation resistance compared with layered YSZ-Al_2O_3 coatings. Pantoja-Pertegal *et al.* [19] prepared EPD suspensions for the coating of stainless steel substrates by dispersing 3 mol% yttria stabilized zirconia (3YSZ) powders in two different solvents, namely isopropanol and acetone. The average particle size of the powders synthesized by sol-gel was in the range of 10–12 μm [19]. However, despite previous research, limited experimental studies have been conducted on nanostructured TBC (NTBC) while offering conflicting data [14].

Inconel 718 is a high-strength metal and one of the nickel-based superalloys extensively utilized in the aerospace industry for the hot sections of gas turbine engines [29]. Therefore, its coating is of great importance for such applications.

One major challenge of the EPD process is to achieve quality by preventing the formation of cracks due to changes in temperature during the drying and sintering of ceramic coatings. Due to the melting and oxidation of aluminium and subsequent *in situ* formation of alumina during the sintering of composite, the process of deposit compaction and bonding can be promoted at relatively low temperatures, which in turn can affect service reliability and mechanical integrity [30] and lead to the formation of crack-free composite coatings [31].

The commonly used sintering temperatures of more than 1200 °C may damage the metal parts and also lead to high production costs [32]. In order to overcome these disadvantages of high sintering temperatures, reaction bonding by Al is suggested [31]. The addition of Al to the green form composites can promote the sintering of the ceramic coatings at relatively low temperatures. The volume shrinkage due to the sintering can be compensated by the volume expansion due to the oxidation of aluminium in the green form coatings eliminating cracking of the coating and a dense ZrO_2/Al_2O_3 coating can be obtained [31,32]. These FGM composites may have applications in the extreme thermal shielding for Inconel 718, and the strong joining of YSZ ceramics to metallic substrate through the help of a metal such as the Al.

The main aim of the current work is thus to characterize the properties of nanostructured YSZ/Al_2O_3 composite TBC with gradient structure made onto Inconel 718 by electrophoretic technique and to overcome the limitations of EPD for creating high thicknesses as well as sintering of YSZ at a low temperature through reaction bonding by Al.

II. Experimental

2.1. Fabrication of graded composite coating

The starting materials applied in this study were: zirconia stabilized with 3 mol% yttria (3%YSZ, >99%, the average particle size of 50 nm, Jiaozuo Huasu Chemical Co. Ltd, China) as the coating material, aluminium powder (>99.5%, PMC, Iran) as the source for *in situ* formation of aluminium oxide and a sintering aid, iron (III) oxide (Fe_2O_3, >99.5%, Alfa Aesar, UK) as another sintering aid and iodine (Merck, Germany) as adjuster of the particles surface charge in suspensions or dispersant.

In the first step, the aluminium powder in the as-received form was subjected to milling for 10 h to make a finer powder, using a ball mill with a rotation speed of 200 rpm under an argon atmosphere at room temperature. The container was made of hardened steel and the balls used in this process were made of stainless steel. The total weight ratio of balls to powder was 1:15. Stearic acid (2 wt.%) was utilized as a process control agent (PCA) to prevent excessive cold welding of powder particles.

Thereafter, 20 ml of ethanol (>99%, Sigma-Aldrich) and acetyl-acetone (ACAC, > 99%, Sigma-Aldrich) mixture with a volume ratio of 1:1 was prepared. The YSZ nanoparticles and aluminium powder with different weight ratios, 0.001 g iodine (0.5 g/l) and iron oxide were dispersed in the prepared mixture to produce suspensions with YSZ/Al total concentration of 20 g/l. In order to prevent agglomeration, the resulting suspension was agitated on a magnetic stirrer apparatus for 45 min and then placed in an ultrasonic bath with a frequency of 35 kHz for 15 min.

The EPD cells contained two Inconel and stainless steel electrodes (with dimensions of $10 \times 10\ mm^2$) at the distance of 10 mm. Electrodes were submerged parallel to each other in suspension. Stainless steel was used as the anode material, whereas the cathode electrode was made of Inconel 718 sheets having 2.5 mm thickness. Before coating, the metallic substrates were washed with detergent and distilled water, degreased with acetone and then dried in air at room temperature. Electrodes were connected to different DC power supplies to generate the driving power required for each layer formation. Three suspensions with different amounts of YSZ and Al (YSZ, YSZ–30 wt.% Al and YSZ–50 wt.% Al) were prepared to produce the thermal barrier FGM coating and the deposition process for each suspension was consecutively performed by changing the voltage, while the values of all other EPD parameters were taken as constant. The first layer was obtained from YSZ–50 wt.% Al suspension, whereas the third layer was pure YSZ (Fig. 1). The detailed description of the preparation conditions for three suspensions is summarized in Table 1.

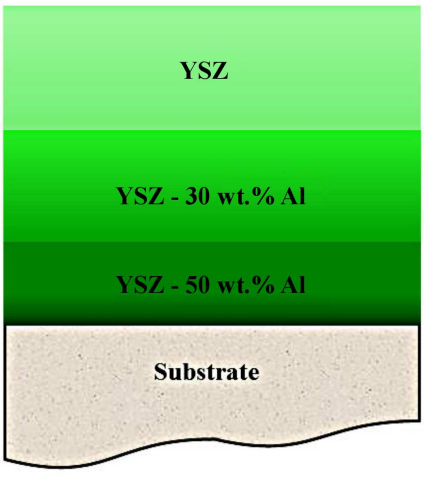

Figure 1. Schematic of achieved functionally graded thermal barrier coating

After drying of each layer, the obtained green graded coating was subjected to heat treatment procedure consisting of three steps. In the first step the dried coating was heated to 660 °C at a rate of 2 °C/min in air and held for 3 h at this temperature to start melting of Al [34]. Aluminium melting increases connections between particles and refines bonding strength, which in turn leads to the suppression of the crack propagation in the coating. This event was followed by the oxidation of aluminium and the subsequent formation of Al_2O_3 as a secondary phase [33]. To increase the formation of alumina, the oxidation procedure was repeated so that the alumina formed in the first step was partially separated from the aluminium particles surface due to the cooling and shrinkage of aluminium. Thus, in the second step of heating, previously formed alumina particles can operate as heterogeneous nucleation sites for the formation of more alumina [34–36]. In the third step, the FGM coating containing Al_2O_3 phase was heated to 1150 °C at a rate of 2 °C/min and kept for 4 h to increase the adhesion and density of the coating. After each step, the coated substrate was allowed to cool down to ambient temperature.

2.2. Electrophoretic mobility

The mobility of particles in suspension can be determined by the Henry equation, where electrophoretic mobility (μ) is dependent on the zeta potential of the particles (ζ), the dielectric constant of the suspending medium (ε) and the viscosity of the suspension (η), as follows [37]:

$$\mu = \frac{2\varepsilon \cdot \varepsilon_0 \cdot \zeta}{3\eta} \cdot f \tag{1}$$

where ε_0 is the vacuum dielectric permittivity and f is the Henry coefficient, which is a function of the product of particle radius (r) in suspensions and the thickness of the electric double layer. For a state where the double layer is thin in comparison with the particle size, the Henry equation can be expressed approximately by the Smoluchowski's mobility formula [38,39]:

$$\mu = \frac{\varepsilon \cdot \varepsilon_0 \cdot \zeta}{\eta} \tag{2}$$

Table 1. Amounts of starting materials and conditions utilized for the deposition of different suspensions

Suspension	YSZ [g/l]	Al [g/l])	I_2 [g/l])	Fe_2O_3 [g/l])	Voltage [V]	Time [s]
YSZ	20	0	0.5	0.16	65	300
YSZ-30 wt.% Al	14	6	0.5	0.16	45	240
YSZ-50 wt.% Al	10	10	0.5	0.16	25	180

2.3. Characterization

In order to evaluate the surface morphology and cross-section view of the coating, the field emission scanning electron microscopy (FE-SEM) images were captured on a Mira3 Tescan (Brno, Czech Republic). Coating morphology was probed by FE-SEM in both in-beam secondary electron and back-scattered electron modes. The coated sample was cut using wire cut electrical discharge machining to examine the microstructural characteristics of the cross-section surfaces using the secondary electron images of FE-SEM. The elemental contents of prepared composites were evaluated by energy dispersive X-ray spectroscopy (EDS) combined with FE-SEM.

The deposited coating was characterized by X-ray diffraction (XRD, Philips PW 1730 by using Cu-K_α radiation) to identify the crystalline phases. Zeta potential and particle size of the suspensions were measured employing a Zeta seizer HS 3000 electrophoretic light scattering instrument (Malvern Ltd, UK). The thermal behaviour of the Al powder was monitored by DTA/TGA (differential thermal analysis/thermo-gravimetric analysis) up to 800 °C with a heating rate of 5 °C/min.

III. Results and discussion

3.1. Particle size and ζ-potential measurements

The colloidal stability of the particles has a significant influence on the deposition rate and the final microstructure of the coatings [8,40]. Previous studies have demonstrated that well-dispersed particles are necessary to produce densely packed deposits [31]. Therefore, Al powder was milled before dispersion, and the size and morphology of the particles before and after milling are shown in Fig. 2. A distinct powder morphology changed from quasi-spherical to fragmented, irregular and flake-like particles as a result of milling. The decrease of the particle size of the milled Al powder is also evidenced but with an inclination to agglomeration. Due to the hardening of the particles, they are prone to the phenomenon of particle fracturing and subsequent refinement.

Ethanol and acetyl-acetone mixture with a volume ratio of 1:1 was used to prepare the suspensions even though it is known that the disadvantage of using a non-aqueous medium is that the particles are more difficult to stabilize [37]. Therefore, the suspensions were prepared by adding iodine as a suspension stabilization agent to help disperse powders and reduce flocculation. The influence of iodine as a stabilizing agent on the surface charge was evaluated. The change of the zeta potential (ζ) of the EPD suspension and the average size distribution of the particles are plotted versus the amount of iodine added to the suspension (Fig. 3). When iodine concentration was changed from 0 to 0.5 g/l, the zeta potential of the suspension increased up to the maximum value of 45.7 mV. On the other hand, the average particle size distribution was simultaneously reduced to the minimum of 232 nm, which is noticed to be the optimum point [41].

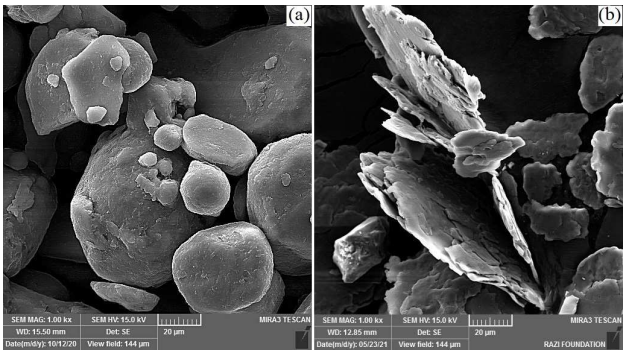

Figure 2. SEM images of samples of pure aluminium powder: (a) before milling and (b) after 10 h milling

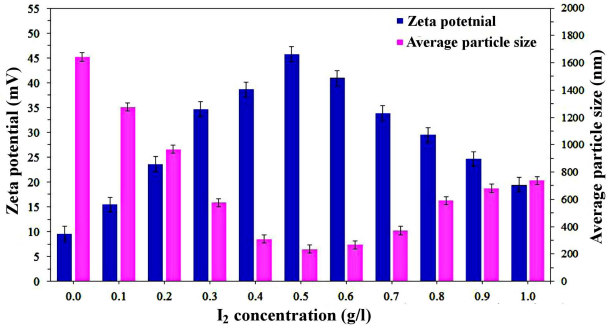

Figure 3. Column chart of zeta potential and average size distribution of particles as functions of iodine added to the suspensions containing the mixture of ethanol-acetylacetone

The initial increase in zeta potential (ζ) with iodine addition can be attributed to the adsorption of formed H^+ ions onto the surface of the particles. These positive ions are generated by reactions between I_2 and acetylacetone as well as I_2 and ethanol [30,42,43]. H^+ concentration seems to increase with an increment in the amount of iodine, and becomes excessive when iodine concentration exceeds 0.5 g/l. By increasing H^+ above its optimum value, the surface charge of particles saturates and the free positive ions that are formed carry some electrical charge, and the corresponding zeta potential declines. Therefore, interparticle electrostatic repulsive force decreases when iodine concentration is not optimum. Consequently, the colloidal stability is reduced and agglomeration of particles is induced [8, 44–46].

3.2. Thermal analysis of aluminium

To understand the behaviour of aluminium powder during sintering, the powder was subjected to DTA/TG thermal analyses and the results are illustrated in Fig. 4. The DTA graph displays an exothermic peak at 638 °C that corresponds to the melting point of aluminium, then an endothermic peak at 690 °C which is associated with the oxidation of aluminium. The TG curve indicates the gradual weight gain from room temperature up to

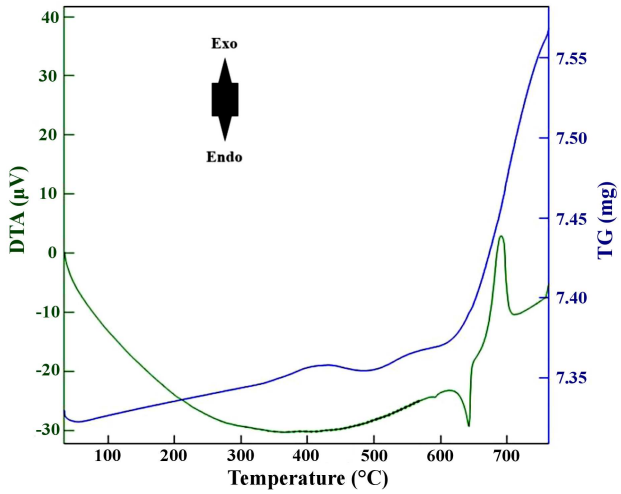

Figure 4. DTA/TG of the Al powder after milling for 10 h

638 °C. Due to the fineness of the aluminium particles, they gradually absorb oxygen and react with oxygen from the air and the weight of the powders increases until it reaches the point of 638 °C. Above this temperature, molten Al quickly reacts with oxygen and strongly oxidizes and forms alumina. This corresponds to the exothermic peak and a very steep slope can be seen up to 800 °C.

With regard to TG trace, Al oxidizes faster at higher temperatures which will eventually increase the surface roughness. Therefore, the results of DTA/TG curves suggest that the green zirconia/Al composite coating should be kept at 660 °C during sintering for some time so that the aluminium present in the coating can slowly be oxidized. Furthermore, at the melting temperature of aluminium, the melt has a chance to diffuse into holes and porosity of the coating, and consequently, the density of the coating will increase before significant oxidation.

3.3. Formation of FGM structure

The electrophoretic deposition method is less costly and more flexible in comparison with the conventional coating techniques for the application of thermal barrier coatings [47]. However, by this method, the thickness of the coating is usually limited to a critical size of 100 μm, which is a restriction for the preparation of thick coatings such as thermal barrier coatings (with a thickness of about 200–400 μm) [48].

In this work, in order to overcome the electrical resistance of non-conductive deposits and provide a suitable thickness for the application in TBCs, after each step of the layer formation, the voltage was increased (voltage is an effective parameter in controlling the thickness of the coating). The applied voltage can be written as [47]:

$$E_0 = \Delta E_{cathode} + \Delta E_{deposit} + \Delta E_{suspension} + \Delta E_{anode} \quad (3)$$

where $\Delta E_{cathode}$, ΔE_{anode}, $\Delta E_{deposit}$ and $\Delta E_{suspension}$ are the voltage drops caused by the polarization of the cathode and anode and the resistance of deposit and suspension, respectively. The velocity of particle motion (v) is given by the following equation [37]:

$$v = \mu \cdot E \quad (4)$$

where E is the intensity of the electric field and μ is the electrophoretic mobility of the particles. According to Eq. 4, increasing the voltage adds the intensity of the electric field, which in turn increases the velocity of the particle's motion [37]. As a result, the thickness of the coating increases.

As deposition proceeds, the increased resistance of the coating drops the voltage in the deposit, while reducing the voltage drop in the suspension. This leads to a reduction in the mobility of the suspended particles driven by the electric field and subsequently decreases the accumulation rate of particles for the formation of an additional layer. By utilizing a gradient voltage rather than a constant voltage, the deposition rate of particles can be maintained at a constant and moderate value [47]. As a result, the coating microstructure may be obtained as uniform and densely packed.

In order to compare the kinetics of layer formation, weights of a single layer obtained by different prepared suspensions under three applied voltages (25, 45 and 65 V) were also individually measured. Figure 5 compares the variation in the weight of a single-layer coating over time with respect to the change in the composition of suspensions at various electric potentials.

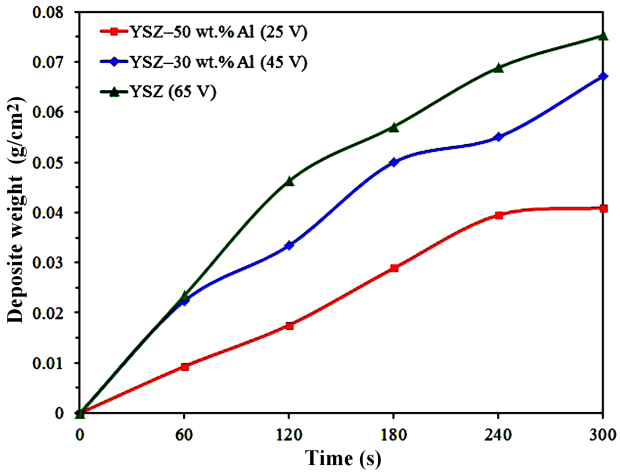

Figure 5. Simultaneous effect of suspension composition and applied fields on the deposit weight of a single-layer coating versus time

Due to the high surface area of nanoparticles, the concentration of electrolyte in the suspension is increased and the zeta potential drops. Consequently a lower deposition rate is expected for suspensions with higher amount of YSZ nanoparticles [49]. Moreover, a more considerable amount of free ions that may be formed in these suspensions will carry some electric charge, which in turn can lead to a decrease in the deposition rate of YSZ [42]. Therefore, it is expected that deposition yields decrease with the relative amount of YSZ

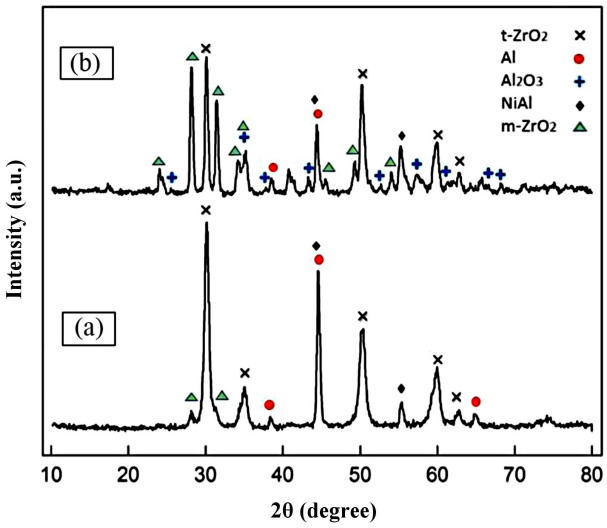

Figure 6. XRD patterns for FGM coating: a) green dried coating and b) after sintering

nanoparticles. Nevertheless, as shown in Fig. 5, the driving force for the electrophoretic deposition is added by increasing the voltage which originates from Coulombic forces applied to the suspended particles within the suspension [50].

3.4. XRD analysis

One major challenge of the EPD process is the sintering of coatings, which is necessary to achieve a stable layer with good mechanical properties. Figure 6 shows the XRD patterns of the FGM sample before any sintering and also after sintering at 1150 °C. The XRD pattern of the created green coating indicates the presence of peaks ascribed to zirconia and aluminium phases. It can be seen that the deposited sample before sintering contains a tetragonal phase as well as a slight amount of monoclinic phase of zirconia [51]. The appearance of the NiAl phase can be assigned to intermetallic compounds of bond coat on Ni-based superalloy substrates [52,53].

The XRD results confirmed the transformation of the starting Al phase into the final Al_2O_3 phase and the formation of the YSZ-Al_2O_3 composite after the sintering. Even though some of the peaks overlapped, it appears that some small amount of Al phase is present in the sintered sample, possibly since the aluminium has not been wholly oxidized yet. More alumina may be expected to be formed with an increase in sintering temperature [54]. However, this is limited by the temperature stability of Inconel 718 applied as substrate [55,56]. Furthermore, the oxidation of aluminium and phase transformation to crystalline alumina could be intensified by adding nanosized alumina particles as nucleation seeds [35]. In addition, it seems that the rise in temperature has influence on partial removal of yttrium from the zirconium oxide and results in the formation of higher amount of monoclinic zirconia (m-ZrO_2) due to the martensitic phase transformation [57].

3.5. Microstructural analysis

Figure 7a illustrates a low-magnification transverse-section FE-SEM micrograph of a typical FGM coating after sintering. The three smooth and crack-free TBC layers fabricated by different steps of the electrophoretic process are evident. It can be observed that the first layer formed at a voltage of 25 V has a thickness of about 53 μm, the second layer created at a voltage of 45 V has a thickness of about 70 μm and the third layer made at a voltage of 65 V has a thickness of 78 μm. Accordingly, based on Eqs. 3 and 4 and by using the increased voltage at each step, the deposit resistance was overcome. Hence, by applying these voltages, the thickness of the coating has reached the thickness required for a TBC.

In-beam secondary electron detector enables us to observe extraordinary sharp surface details and highlights topography. In this way, Fig. 7b shows the surface morphology of the FGM coating through a high-magnification micrograph, which reveals that the YSZ nanoparticles predominantly exist in the final layer. The occurrence of necking between particles is due to the

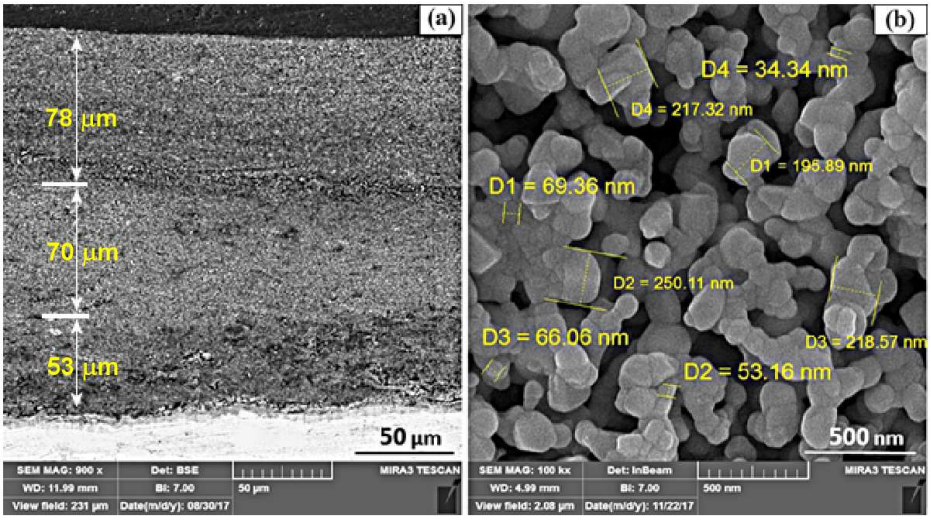

Figure 7. FESEM micrographs of: a) cross-section and b) surface morphology of graded YSZ/Al_2O_3 composite coating

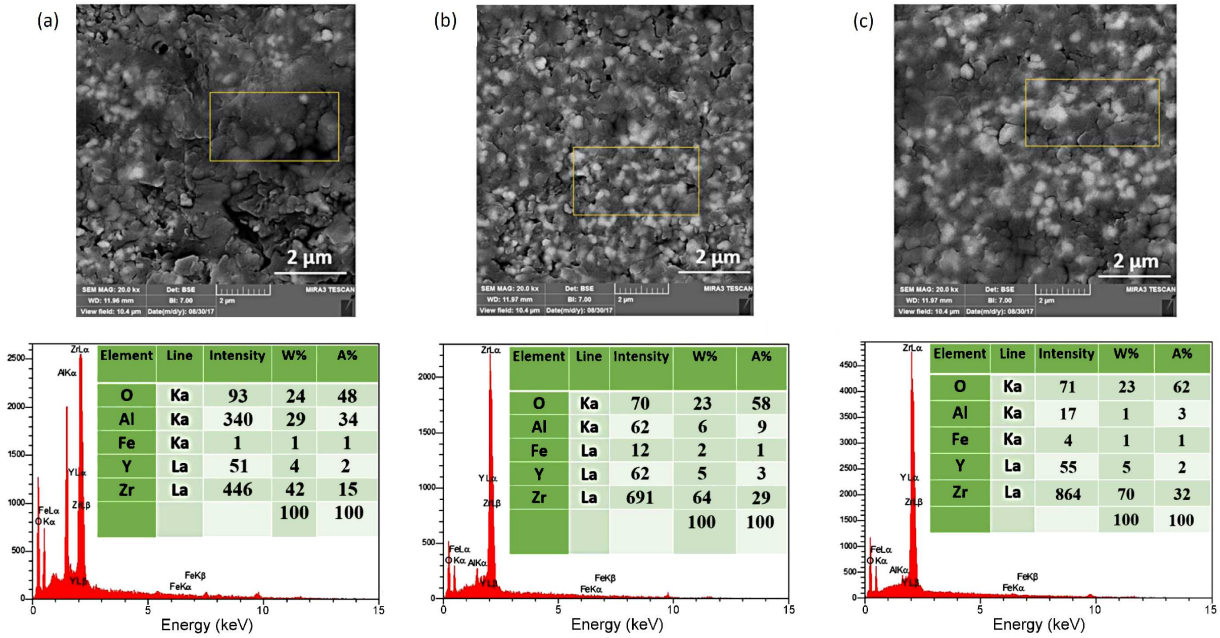

Figure 8. FESEM images and typical EDS spectra of selected area at the cross-section of FGM coating: a) first, b) second and c) third layer

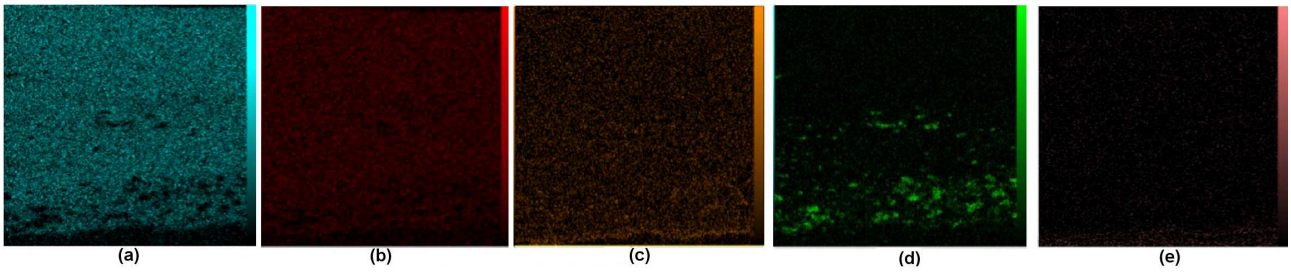

Figure 9. The elemental EDS mapping pattern from a cross-sectional view (thickness) of the FGM coating: a) Zr (blue), b) Y (red), c) O (orange), d) Al (green) and e) Fe (pink)

sintering and diffusion that have been driven by the desire of the particle to minimize the energy [58].

3.6. EDS analysis

In order to demonstrate the formation of the FGM coating, the elemental composition of each layer was characterized by EDS spectra of the selected area, as represented in Fig. 8. Based on the results of the EDS obtained from the cross-section of each layer, it is observed that the weight percent of aluminium gradually reduces from the first to the third layer while zirconium amount increases, as expected.

To understand the distribution of the elements along the thickness direction, EDS mapping is displayed in Fig. 9. It is evident that blue, red, orange, green and pink dots related to the Zr, Y, O, Al and Fe elements, respectively, exist at the cross-section area of the coating. According to elemental distribution presented in Fig. 9 it is observed that the amount of aluminium in the first layer of the coating is higher than that in other layers. In contrast, the zirconium content in the third layer is the highest. The presence of Fe can be attributed to Fe_2O_3 added to EPD suspension as a sintering aid. However, there is probability that Fe diffuses from the substrate into the bottom layer of the coating [59].

It can be also seen (Fig. 9d) that aluminium exists in the form of agglomerates. The non-homogeneous distribution of Al element in the bottom layers may be caused by the difference in the electrophoretic mobility (μ) of Al and YSZ particles in suspension which were obtained as 0.903 and 0.581 cm^2/Vs, respectively. According to previous studies, the higher electrophoretic mobility of Al makes it easier to move and deposit on the electrode. In the second layer, due to the lower aluminium content in the suspension and coating, the agglomeration is less pronounced. Furthermore, in the early stages of layer formation, the particles that have more mobility are deposited faster, and thereafter depletion of these particles in suspension occurs, and consequently, the amount of these particles for layer formation declines as the deposition proceeds [60]. In addition, to form the first layer, a composite suspension containing a high concentration of Al (micron-sized) particles and YSZ (nanoparticles) was made. As the thickness of the electrical double layer reduces around the micron-sized particles, zeta potential approaches zero

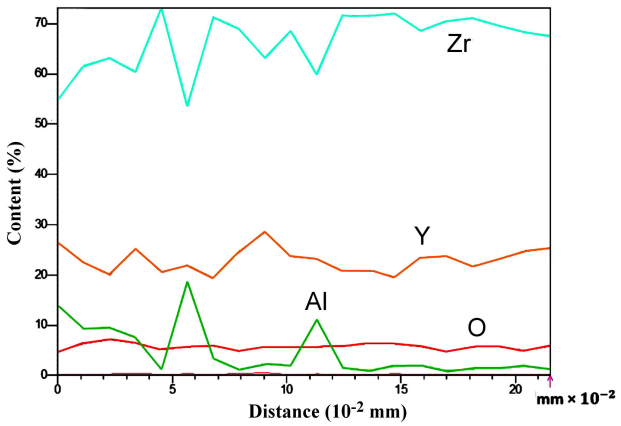

Figure 10. Line scan of EDS analysis along a cross-section of FGM coating

and the electrostatic repulsion forces between these particles decrease and eventually cause the particles to stick together and deposit [41,61,62].

Figure 10 represents the line scan of EDS analysis performed in twenty points along a single line. The general trend of changes indicates that by moving away from the substrate, the amounts of Zr were found to increase gradually across the cross-section of the coating while the Al element value decreased. The appearance of the peaks on the graph may be due to the agglomerate formation in some regions. In fact, achieving stable, non-agglomerated suspensions is particularly difficult if nanosized powders are used because remarkable interfacial interactions lead to a strong agglomeration tendency [63,64]. Moreover, the application of an electric field favours the tendency for agglomeration, and consequently, rapid sedimentation of the suspended particulates takes place [19,46].

IV. Conclusions

Suspensions including different amounts of nanosized YSZ along with Al particles as the secondary phase and reactive bonding agent were co-deposited consecutively on Inconel 718 substrate. Three-layer YSZ/Al_2O_3 coating with a compositional gradient (concentration of YSZ increased gradually from the substrate to the surface) was successfully obtained by using a multi-step electrophoretic technique followed by sintering. To prepare the functionally graded thermal barrier coating with desirable thickness, the fabrication of each layer was performed by changing the voltage and suspension composition, while keeping other EPD parameters constant. Thus, the first, second and third layers reached thicknesses of about 53, 70 and 78 μm, respectively.

XRD analysis indicated that tetragonal zirconia, monoclinic zirconia and alumina are main phases in the coating sintered at 1150 °C. However, a small amount of Al phase is also present in the coating, possibly since it has not been fully oxidized. The EDX mapping patterns revealed the presence of Zr, Al, Fe, O and Y elements, while Al content in the first layer of the coating is higher than that in other layers. In contrast, the zirconium content in the third layer is the highest.

The obtained results suggested that EPD is an effective method for fabricating functionally graded TBCs with suitable thicknesses at lower sintering temperatures. For the formation of FGM with more layers, the use of ultra-fine aluminium particles and the addition of nanosized alumina particles as nucleation seeds can be accounted for future trends of this investigation.

Acknowledgements: The authors would like to thank Islamic Azad University, Takestan Branch, for the financial support provided for the internal research work.

References

1. K.K. Chawla, *Ceramic Matrix Composites*, 2nd Edition, Springer, New York, 2014.
2. R.W. Steinbrech, "Toughening mechanisms for ceramic materials", *J. Eur. Ceram. Soc.*, **10** (1992) 131–142.
3. L. Cheng, M. Sun, F. Ye, Y. Bai, M. Li, S. Fan, L. Zhang, "Structure design, fabrication, properties of laminated ceramics: A review", *Int. J. Lightweight Mater. Manufact.*, **1** (2018) 126–141.
4. F.D. Minatto, P. Milak, A. De Noni, D. Hotza, O.R.K. Montedo, "Multilayered ceramic composites – A review", *Adv. Appl. Ceram.*, **114** (2015) 127–138.
5. V. Bhavar, P. Kattire, S. Thakare, S. Patil, R.K.P. Singh, "A review on functionally gradient materials (FGMs) and their applications", *IOP Conf. Series Mater. Sci. Eng.*, **229** (2017) 012021.
6. P. Hvizdoš, D. Jonsson, M. Anglada, G. Anné, O. Van Der Biest, "Mechanical properties and thermal shock behaviour of an alumina/zirconia functionally graded material prepared by electrophoretic deposition", *J. Eur. Ceram. Soc.*, **27** (2007) 1365–1371.
7. S. Hu, W. Li, H. Finklea, X. Liu, "A review of electrophoretic deposition of metal oxides and its application in solid oxide fuel cells", *Adv. Colloid Interf. Sci.*, **276** (2020) 102102.
8. S. Cabanas-Polo, A.R. Boccaccini, "Electrophoretic deposition of nanoscale TiO_2: Technology and applications", *J. Eur. Ceram. Soc.*, **36** (2016) 265–283.
9. I. Corni, M.P. Ryan, A.R. Boccaccini, "Electrophoretic deposition: From traditional ceramics to nanotechnology", *J. Eur. Ceram. Soc.*, **28** (2008) 1353–1367.
10. U.V. Akhil, N. Radhika, L. Rajeshkumar, G. Sivaswamy, "A comprehensive review on ceramic coating on steel and centrifugal thermite process: Applications and future trends", *J. Bio-Tribo-Corrosion*, **9** (2023) 41.
11. P.K. Dubois, A. Gauvin-Verville, B. Picard, J.-S. Plante, M. Picard, "Thermal barrier coating applied to the structural shroud of an inside-out ceramic turbine", in *ASME Turbo Expo 2021: Turbomachinery Technical Conference and Exposition*, Ed., 2021.
12. Q. Liu, S. Huang, A. He, "Composite ceramics thermal barrier coatings of yttria stabilized zirconia for aero-engines", *J. Mater. Sci. Technol.*, **35** (2019) 2814–2823.
13. A.G. González-Hernández, H. Ageorges, M.E. López, "Microstructural evaluation of YSZ/NiCrAlCo-Y_2O_3 coatings after isothermal oxidation at 1050°C", *J. Phys. Conf. Series*, **1119** (2018) 012017.

14. A. Kumar, J. Moledina, Y. Liu, K. Chen, P.C. Patnaik, "Nano-micro-structured 6%–8% YSZ thermal barrier coatings: A comprehensive review of comparative performance analysis", *Coatings*, **11** (2021) 1474.
15. S. Ariharan, A. Nisar, N. Balaji, S.T. Aruna, K. Balani, "Carbon nanotubes stabilize high temperature phase and toughen Al_2O_3-based thermal barrier coatings", *Composites Part B Eng.*, **124** (2017) 76–87.
16. P. Wang, Y.-D. He, S.-J. Deng, J. Zhang, "Porous α-Al_2O_3 thermal barrier coatings with dispersed Pt particles prepared by cathode plasma electrolytic deposition", *Int. J. Minerals Metal. Mater.*, **23** (2016) 92–101.
17. S.-K. Jia, Y. Zou, J.-Y. Xu, J. Wang, L. Yu, "Effect of TiO_2 content on properties of Al_2O_3 thermal barrier coatings by plasma spraying", *Trans. Nonferrous Metals Soc. China*, **25** (2015) 175–183.
18. K.T. Pasupuleti, K. Vattappara, S.A. Gomes, P. Ramaswamy, "Thermal fatigue characteristics of $8Y_2O_3$-ZrO_2, $La_2Zr_2O_7$, La_2 $(Zr_{0.7}Ce_{0.3})_2O_7$ and $La_2Ce_2O_7$ thermal barrier coatings in duplex, multilayer functionally graded and multilayer configurations", *Process. Appl. Ceram.*, **17** (2023) 236–247.
19. J.L. Pantoja-Pertegal, A. Díaz-Parralejo, A. Macías-García, J. Sánchez-González, E.M. Cuerda-Correa, "Design, preparation, and characterization of yttria-stabilized zirconia (YSZ) coatings obtained by electrophoretic deposition (EPD)", *Ceram. Int.*, **47** (2021) 13312–13321.
20. B. Basu, K. Balani, *Advanced Structural Ceramics*, Wiley, 2011.
21. S. Goel, S. Björklund, N. Curry, G.S.U. Wiklund, C. Gaudiuso, S. Joshi, "Axial plasma spraying of mixed suspensions: A case study on processing, characteristics, and tribological behavior of Al_2O_3-YSZ coatings", *Appl. Sci.*, **10** (2020) 5140.
22. M.S. Ahmadi, R. Shoja-Razavi, Z. Valefi, H. Jamali, "Evaluation of hot corrosion behavior of plasma sprayed and laser glazed YSZ-Al_2O_3 thermal barrier composite", *Optics Laser Technol.*, **111** (2019) 687–695.
23. A. Keyvani, M. Saremi, M. Heydarzadeh Sohi, Z. Valefi, M. Yeganeh, A. Kobayashi, "Microstructural stability of nanostructured YSZ–alumina composite TBC compared to conventional YSZ coatings by means of oxidation and hot corrosion tests", *J. Alloys Compd.*, **600** (2014) 151–158.
24. L. Sun, A. Sneller, P. Kwon, "Fabrication of alumina/zirconia functionally graded material: From optimization of processing parameters to phenomenological constitutive models", *Mater. Sci. Eng. A*, **488** (2008) 31–38.
25. P. Sarkar, X. Huang, P.S. Nicholson, "Zirconia/alumina functionally gradiented composites by electrophoretic deposition techniques", *J. Am. Ceram. Soc.*, **76** (1993) 1055–1056.
26. F. Kirbiyik, M.G. Gok, G. Goller, "Microstructural, mechanical and thermal properties of Al_2O_3/CYSZ functionally graded thermal barrier coatings", *Surface Coatings Technol.*, **329** (2017) 193–201.
27. R. Liu, S. Yuan, Z. Wang, Y. Zhao, M. Zhang, L. Shi, "Graded YSZ/Al_2O_3 hot corrosion resistant coating with enhanced thermal shock resistance", *RSC Advances*, **3** (2013) 17034–17038.
28. M. Saremi, Z. Valefi, "Thermal and mechanical properties of nano-YSZ-alumina functionally graded coatings deposited by nano-agglomerated powder plasma spraying", *Ceram. Int.*, **40** (2014) 13453–13459.
29. A.R.C. Sharman, J.I. Hughes, K. Ridgway, "Workpiece surface integrity and tool life issues when turning Inconel 718™ nickel based superalloy", *Machin. Sci. Technol.*, **8** (2004) 399–414.
30. O. Khanali, S. Baghshahi, M. Rajabi, "Fabrication and characterization of YSZ/Al_2O_3 nano-composite coatings on Inconel by electrophoretic deposition", *J. Mater. Res.*, **32** (2017) 3402–3408.
31. Z. Wang, J. Shemilt, P. Xiao, "Fabrication of ceramic composite coatings using electrophoretic deposition, reaction bonding and low temperature sintering", *J. Eur. Ceram. Soc.*, **22** (2002) 183–189.
32. B. Baufeld, O. van der Biest, H.-J. Rätzer-Scheibe, "Lowering the sintering temperature for EPD coatings by applying reaction bonding", *J. Eur. Ceram. Soc.*, **28** (2008) 1793–1799.
33. E. Karimi, J. Khalil-Allafi, V. Khalili, "Electrophoretic deposition of double-layer HA/Al composite coating on NiTi", *Mater. Sci. Eng. C*, **58** (2016) 882–890.
34. M. Nicoara, C. Locovei, C. Opris, D. Ursu, R. Vasiu, M. Stoica, "Optimizing the parameters for in situ fabrication of hybrid Al-Al_2O_3 composites", *J. Therm. Anal. Calorim.*, **127** (2017) 115–122.
35. F.S. Yen, H.S. Lo, H.L. Wen, R.J. Yang, "θ- to α-phase transformation subsystem induced by α-Al_2O_3-seeding in boehmite-derived nano-sized alumina powders", *J. Crystal Growth*, **249** (2003) 283–293.
36. J. Liu, F. Verhaeghe, M. Guo, B. Blanpain, P. Wollants, "In situ observation of the dissolution of spherical alumina particles in CaO-Al_2O_3-SiO_2 melts", *J. Am. Ceram. Soc.*, **90** (2007) 3818–3824.
37. K. Maca, H. Hadraba, J. Cihlar, "Electrophoretic deposition of alumina and zirconia: I. Single-component systems", *Ceram. Int.*, **30** (2004) 843–851.
38. H. Ohshima, "Approximate analytic expression for the electrophoretic mobility of a spherical colloidal particle", *J. Colloid Interface Sci.*, **239** (2001) 587–590.
39. H. Ohshima, T. Kondo, "On the electrophoretic mobility of biological cells", *Biophys. Chem.*, **39** (1991) 191–198.
40. A. Szydło, J.-D. Goossen, C. Linte, H. Uphoff, M. Bredol, "Preparation of platinum-based electrocatalytic layers from catalyst dispersions with adjusted colloidal stability via a pulsed electrophoretic deposition method", *Mater. Chem. Phys.*, **242** (2020) 122532.
41. M. Kari, M. Montazeri-Pour, M. Rajabi, V. Tizjang, S. Moghadas, "Maximum SiO_2 layer thickness by utilizing polyethylene glycol as the surfactant in synthesis of core/shell structured TiO_2-SiO_2 nano-composites", *J. Mater. Sci. Mater. Electron.*, **25** (2014) 5560–5569.
42. T. Ishihara, K. Shimose, T. Kudo, H. Nishiguchi, T. Akbay, Y. Takita, "Preparation of yttria-stabilized zirconia thin films on strontium-doped $LaMnO_3$ cathode substrates via electrophoretic deposition for solid oxide fuel cells", *J. Am. Ceram. Soc.*, **83** (2000) 1921–1927.
43. S.Y. Ng, A.R. Boccaccini, "Lead zirconate titanate films on metallic substrates by electrophoretic deposition", *Mater. Sci. Eng. B*, **116** (2005) 208–214.
44. V. Tizjang, M. Montazeri-Pour, M. Rajabi, M. Kari, S. Moghadas, "Surface modification of sol-gel synthesized TiO_2 photo-catalysts for the production of core/shell structured TiO_2-SiO_2 nano-composites with reduced photo-

catalytic activity", *J. Mater. Sci. Mater. Electron.*, **26** (2015) 3008–3019.
45. M. Montazeri-Pour, N. Riahi-Noori, A. Mehdikhani, "Synthesis of single-phase anatase TiO_2 nanoparticles by hydrothermal treatment with application potential for photoanode electrodes of dye sensitized solar cells", *J. Ceram. Process. Res.*, **14** (2013) 595–600.
46. D. Das, B. Bagchi, R.N. Basu, "Nanostructured zirconia thin film fabricated by electrophoretic deposition technique", *J. Alloys Compd.*, **693** (2017) 1220–1230.
47. M. Bai, F. Guo, P. Xiao, "Fabrication of thick YSZ thermal barrier coatings using electrophoretic deposition", *Ceram. Int.*, **40** (2014) 16611–16616.
48. X.Q. Cao, R. Vassen, D. Stoever, "Ceramic materials for thermal barrier coatings", *J. Eur. Ceram. Soc.*, **24** (2004) 1–10.
49. H. Farnoush, J. Aghazadeh Mohandesi, D. Haghshenas Fatmehsari, F. Moztarzadeh, "A kinetic study on the electrophoretic deposition of hydroxyapatite–titania nanocomposite based on a statistical approach", *Ceram. Int.*, **38** (2012) 6753–6767.
50. B. Ferrari, R. Moreno, "EPD kinetics: A review", *J. Eur. Ceram. Soc.*, **30** (2010) 1069–1078.
51. S. Taghi-Ramezani, Z. Valefi, M. Mirjani, R. Ghasemi, "The influence of pyrolysing Al_2O_3 precursor on the high temperature properties of the YSZ-Al_2O_3 composite coating", *Surf. Eng.*, **37** (2021) 991–1001.
52. X. Fan, L. Zhu, W. Huang, "Investigation of NiAl intermetallic compound as bond coat for thermal barrier coatings on Mg alloy", *J. Alloys Compd.*, **729** (2017) 617–626.
53. X. Peng, W. Li, L. B. Fu, Y. T. Li, S. M. Jiang, J. Gong, C. Sun, "Role of Re in NiAl bond coating on isothermal oxidation behavior of a thermal barrier coating system at 1100 °C", *Corrosion Sci.*, **218** (2023) 111151.
54. G. Dirras, J. Gubicza, D. Tingaud, S. Billard, "Microstructure of Al-Al_2O_3 nanocomposite formed by in situ phase transformation during Al nanopowder consolidation", *Mater. Chem. Phys.*, **129** (2011) 846–852.
55. S. Sui, Z. Li, C. Zhong, Q. Zhang, A. Gasser, J. Chen, Y. Chew, G. Bi, "Laves phase tuning for enhancing high temperature mechanical property improvement in laser directed energy deposited Inconel 718", *Composites Part B Eng.*, **215** (2021) 108819.
56. A.A. Popovich, V.S. Sufiiarov, I.A. Polozov, E.V. Borisov, "Microstructure and mechanical properties of Inconel 718 produced by SLM and subsequent heat treatment", *Key Eng. Mater.*, **651-653** (2015) 665–670.
57. M. Ramesh, K. Marimuthu, P. Karuppuswamy, L. Rajeshkumar, "Microstructure and properties of YSZ-Al_2O_3 functional ceramic thermal barrier coatings for military applications", *Boletín Soc. Española Cerám. Vidrio*, **61** (2022) 641–652.
58. M.R. Mazlan, N.H. Jamadon, A. Rajabi, A.B. Sulong, I.F. Mohamed, F. Yusof, N.A. Jamal, "Necking mechanism under various sintering process parameters - A review", *J. Mater. Res. Technol.*, **23** (2023) 2189–2201.
59. M. Mrdak, M. Rakin, B. Medjo, N. Bajić, "Experimental study of insulating properties and behaviour of thermal barrier coating systems in thermo cyclic conditions", *Mater. Design*, **67** (2015) 337–343.
60. L. Besra, M. Liu, "A review on fundamentals and applications of electrophoretic deposition (EPD)", *Prog. Mater. Sci.*, **52** (2007) 1–61.
61. A. Araghi, M.J. Hadianfard, "Fabrication and characterization of functionally graded hydroxyapatite/TiO_2 multilayer coating on Ti-6Al-4V titanium alloy for biomedical applications", *Ceram. Int.*, **41** (2015) 12668–12679.
62. H. Simunkova, P. Pessenda-Garcia, J. Wosik, P. Angerer, H. Kronberger, G.E. Nauer, "The fundamentals of nano- and submicro-scaled ceramic particles incorporation into electrodeposited nickel layers: Zeta potential measurements", *Surf. Coat. Technol.*, **203** (2009) 1806–1814.
63. M. Montazeri-Pour, A. Ataie, "Synthesis of nanocrystalline barium ferrite in ethanol/water media", *J. Mater. Sci. Technol.*, **25** (2009) 465–469.
64. F. Parast, M. Montazeri-Pour, M. Rajabi, F. Bavarsiha, "Comparison of the structural and photo-catalytic properties of nanostructured Fe_3O_4/TiO_2 core-shell composites synthesized by ultrasonic and Stöber methods", *Sci. Sinter.*, **52** (2020) 415–432.